Meshfree, sequentially linear analysis of concrete

A. Salam Al-Sabah[1] and Debra F. Laefer[2]

Abstract:

New meshfree method employing the Node-based Smoothed Point Interpolation Method (NS-PIM) is presented as an alternative to the non-linear finite element approach for concrete members. The non-linear analysis is replaced by sequentially linear analyses (SLA), and smeared, fixed concrete cracking model was used. A notched concrete beam was employed for validation. Using a crack band width factor of 2.0 and a 10 mm nodal spacing, the peak load differed by only 3.5% from experimental ones. Overall results were similar to experimental ones, as well as to those published by researchers using finite element SLA. The approach provides two major advantages over finite element-based SLA: (1) nodal distortion insensitivity and (2) nodal spacing insensitivity.

Introduction

The finite element method (FEM) is the most widely used numerical method to study linear and non-linear behaviour (for both materials and geometric components) of structures. The method, in its application to non-linear structural analysis, has matured sufficiently to be the basis of many commercial software packages (ANSYS, Abacus, ATINA, etc.). Despite significant progress in its theoretical and numerical aspects, some weaknesses persist. These can be summarised as follows:

[1] A. Salam Al-Sabah, Ph.D., Research Scientist, Urban Modelling Group, School of Civil, Structural and Environmental Engineering, University College Dublin, Newstead, room G67, Belfield, Dublin 4, Ireland, salam.al-sabah@ucd.ie

[2] Debra F. Laefer, Ph.D., Professor, Head Urban Modelling Group, School of Civil, Structural and Environmental Engineering, University College Dublin, Newstead, room G25, Belfield, Dublin 4, Ireland, debra.laefer@ucd.ie (corresponding author)

- Results are mesh-dependent, with good results requiring a high quality mesh and each element's geometry satisfying shape and aspect ratio limits.
- Models are stiffer than the actual structures. Hence, displacements are underestimated.
- In analysis of geometric non-linearity, elements can become distorted sufficiently to compromise output accuracy.
- Crack propagation usually requires re-meshing, and the robustness of automatic re-meshers is questionable, particularly in three-dimensional problems.

Modelling of reinforced concrete is an important topic, as it is one of the most widely used composite materials in construction. Predicting its behaviour is complicated by factors such as reinforcement yielding, non-linear reinforcement-concrete bond behaviour, non-linear behaviour of concrete in compression, and tension cracking of the concrete. This last aspect contributes most significantly to the early, non-linear behaviour of reinforced concrete beams and slabs. The application of non-linear FEM in the analysis of reinforced concrete structures can be traced back to the 1960s when the first reinforced concrete finite element model which includes the effect of cracking was developed by Ngo and Scordelis (1967).

When loaded in tension, concrete fails suddenly after reaching its tensile limit. The heterogeneous nature of concrete results in a quasi-brittle behaviour that is greatly affected by softening damage (Bazant and Jirásek 2002). To represent this, several fracture models have been proposed as summarized by Rots and Blaauwendraad (1989). An important component of these models is the Fracture Process Zone (FPZ), defined as the zone ahead of the crack tip in which concrete undergoes softening behaviour due to microcracking. Two widely used cracking models are the Fictitious (or cohesive) Crack Model (FCM) introduced by Hillerborg et al. (1976), and Crack Band Model (CBM) as proposed by Bazant and Oh (1983). In the first model, the FPZ is represented as a fictitious line that can transmit normal stress. Fracture energy is then expressed as a function of critical crack separation (or opening width, w) (Bazant and Jirásek 2002). In the CBM, fracturing is modelled as a band of parallel, densely distributed microcracks in the FPZ that has a certain width, which is referred to as the crack band width (Bazant and Oh 1983). The average strain over the FPZ can be related to its deformation through the crack band width. The fracture energy can then be represented as a function of a stress-strain curve and the crack band width.

Concrete fracture models, combined with non-linear models for concrete and steel are typically combined with the FEM to produce numerical procedures for non-linear analysis of reinforced concrete. Early efforts to overcome this encountered two main challenges. The first was the numeric instability due to tensile cracking. The second related to the softening portion of the behaviour. The first was solved by adopting the incremental-iterative solution method (Crisfield 1996), where the unbalanced forces were allowed to dissipate through solution iterations. Since the second resulted from the negative tangent stiffness of the softening part of behaviour, it generated an unstable equilibrium with associated numerical issues in solving the stiffness equation. To surmount this, several methods were initially proposed to control the load or the displacement (Crisfield 1996). Prominent amongst these were the arc length method (Crisfield 1996; Riks 1979) and its variations, the minimum residual displacement method (Chan 1988), and the line search method (Crisfield 1996). Yet challenges remained. These non-linear solution methods required the specification of many control parameters, which depended upon user experience and did not guarantee convergence. Inherent to this are expectations that the user is a highly knowledgeable and experienced practitioner and that the results are obtained after many mesh and parameter refinement attempts. This is particularly true for concrete, where the sudden release of strain energy due to tensile cracking can cause the numerical solution to fail. As such, the aim of this paper was to implement an alternative to non-linear FEM in its application to concrete members.

Methodology

The following paragraphs describe the background and details of the particular meshfree method adopted for this analysis, as well as the sequentially linear analysis method that was employed.

Mesh free methods

When the FEM was introduced in the 1950s, the most widely used numerical method for solving differential equations was the finite difference method (Courant et al. 1967). This strong-form method had a simple mathematical foundation and was easy to implement numerically. The main previous limitation was the need for a regular grid of points to define the analysis domain. These limitations added to the general acceptance of the FEM as a better and more flexible alternative. Although further research related to finite difference overcame the necessity of a regular grid (Liszka and Orkisz 1980), the FEM came to dominate popular usage because of its ability to define complicated geometries, its basis on a robust mathematical foundation, and its ease in conducting error analyses (Thomée 2001).

A fundamental alternative came in the form of meshfree methods. The first member of the group was the Smoothed-Particle Hydrodynamics (SPH) (Gingold and Monaghan 1977; Lucy 1977) in 1977, which was initially applied in solving astrophysical problems. Since then, multiple meshfree methods have been proposed (e.g. Li and Mulay 2013; Liu 2009). These vary in their formulation procedure (strong, weak, weakened weak, or boundary integral) and their local function approximations (moving least square, integral, differential, point, or partition of unity). Despite its name, most meshfree methods still require background cells to conduct the numerical integration of the system matrices. However, the meshfree methods that are based on a strong formulation (e.g. the irregular finite difference method, the finite point method, and local point collocation methods) do not usually require background cells. Unfortunately, most of these methods suffer from reduced accuracy and instability due to node irregularity (Atluri and Zhu 1998; Liu 2009).

In the work presented herein, a special meshfree Point Interpolation Method (PIM) called the meshfree Node-based Smoothed Point Interpolation Method (meshfree NS-PIM) is used. The method was first developed by Liu et al. (2005) under the name Linearly Conforming Point Interpolation Method (LC-PIM). This was later changed to the Nodal Smoothing Operation (2009) to distinguish it from the Edge-based Smoothed Point Interpolation Methods (ES-PIM). Further details on NS-PIM are presented by Liu and Zhang (2013).

Meshfree NS-PIM was formulated using polynomial basis functions that have the Kronecker delta function property, which allowed straightforward implementation of the essential boundary conditions. Furthermore, the Generalized Smoothed Galerkin (GS-Galerkin) weak form was used, which allowed use of incompatible assumed displacement functions. The method is linearly conforming, with upper bound results that are free from volumetric locking (Liu, 2009).

In NS-PIM, as in PIM, the displacement, u^h, of any domain point, x, is approximated using a shape (interpolation) function, $\Phi_I(\mathbf{x})$. This function operates within a small local domain around x (the support domain). The function interpolates the nodal displacement, u_I, of the nodes within the support domain of x (or the support nodes, S_n):

$$u^h(\mathbf{x}) = \sum_{I \in S_n} \Phi_I(\mathbf{x}) u_I \tag{1}$$

The choice of the support domain size and location relative to x, explicitly influence the shape function's ability to interpolate accurately between nodal displacements. If the support domain has a poor arrangement of support nodes, inaccurate interpolation results will be produced. Different schemes were introduced to resolve this issue. In the research presented herein, the T3-scheme (Liu 2009) was adopted, Fig. 1. In that scheme, the background cells that are required to conduct the meshfree weak form integration are used for support node selection. The cells can be generated by triangulating between the nodes. Any point inside a triangle is surrounded by three nodes. This allows the construction of a linear shape function that will result in a constant strain approximation. In this work Delaunay triangulation was used to generate the triangulated support domain used for the T3-scheme.

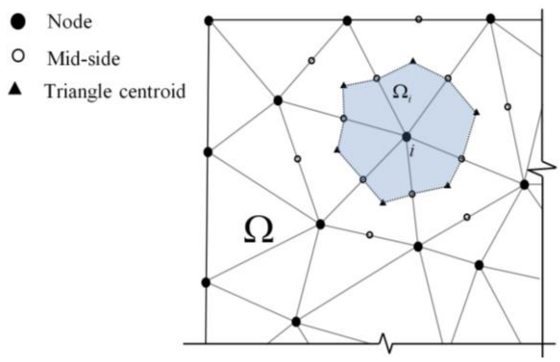

Fig. 1. T-3 scheme for background cells.

The triangulated problem domain (Ω) is divided into a number of smoothing domains (N_s), each centred on a node. As such, N_s equals the number of nodes. The boundaries of smoothing domains do not overlap and have no gaps in between; hence they cover the whole domain.

The Generalized Smoothed Galerkin (GS-Galerkin) weak form, as shown in Eq. (2), can be converted to its discretized form, as shown in Eq. (3), where the domain integration is converted into a summation, thereby adding the effect over the smoothing domains (Liu 2009):

$$\int_{\Omega} \delta\bar{\boldsymbol{\varepsilon}}^{T}\mathbf{c}\bar{\boldsymbol{\varepsilon}}(\mathbf{u})d\Omega - \int_{\Omega}\delta\mathbf{u}^{T}\mathbf{b}d\Omega - \int_{\Gamma_t}\delta\mathbf{u}^{T}\mathbf{t}d\Gamma = 0 \tag{2}$$

$$\sum_{i=1}^{Ns} A_i^s(\delta\bar{\boldsymbol{\varepsilon}}_i)^T\mathbf{c}\bar{\boldsymbol{\varepsilon}}_i - \int_{\Omega}\delta\mathbf{u}^{T}\mathbf{b}d\Omega - \int_{\Gamma_t}\delta\mathbf{u}^{T}\mathbf{t}d\Gamma = 0 \tag{3}$$

where:

$\bar{\boldsymbol{\varepsilon}}_i$: smoothed strain of domain i

A_i^s : area of smoothing domain i

$\mathbf{c}$: material property matrix

$\mathbf{b}$: body force vector

Ω : domain bounded by Γ

t: boundary stress vector

N_s : number of smoothing domains

The smoothed strain $\bar{\boldsymbol{\varepsilon}}$ for node i, Fig. 1, can be found as the approximate strain $\tilde{\boldsymbol{\varepsilon}}(\mathbf{u}^h)$ averaged over the smoothing domain of the node, Ω_i^s, as follows:

$$\bar{\boldsymbol{\varepsilon}}(\mathbf{x}_i) = \frac{1}{A_i^s}\int_{\Omega_i^s}\tilde{\boldsymbol{\varepsilon}}(\mathbf{u}^h)d\Omega \tag{4}$$

The assumed displacement $\mathbf{u}^h(\mathbf{x})$ can be used to find the smoothed strain matrix $\bar{\mathbf{B}}_I$, with its elements representing the smoothed shape function derivatives:

$$\overline{\mathbf{B}}_I(x_i) = \begin{bmatrix} \bar{\phi}_{I,x}(x_i) & 0 \\ 0 & \bar{\phi}_{I,y}(x_i) \\ \bar{\phi}_{I,y}(x_i) & \bar{\phi}_{I,x}(x_i) \end{bmatrix} \tag{5}$$

This matrix can be used to find the approximate smoothed strain (Liu 2009):

$$\bar{\boldsymbol{\varepsilon}}^h(\mathbf{x}_i) = \sum_{I \in S_s} \overline{\mathbf{B}}_I(\mathbf{x}_i)\mathbf{u}_I \tag{6}$$

where:

S_s : support nodes of the smoothing domain that are used in the interpolation

The numeric integration required to calculate the smoothed strain matrix $\bar{B}_I$ resulting from the linear shape function can be conducted using one integration point. The integration can be altered from an area to a line integration using Green's theorem (Thomas et al. 2004). This allows for a more efficient closed-form numerical implementation of the integration.

As in the FEM approach, the stiffness matrix is obtained from the strain matrix as follows:

$$\overline{\mathbf{K}} = \sum_{i=1}^{N_s} A_i^s \overline{\mathbf{B}}^T \mathbf{c} \overline{\mathbf{B}} \tag{7}$$

In the research presented herein, the background triangular cells are generated using a Delaunay triangulation. Once the nodal stiffness matrices are calculated, the global stiffness matrix can be assembled. In meshfree NS-PIM, the boundary conditions can be applied explicitly, in a manner similar to the normal procedure in FEM. The overall solution steps are also similar to those applied in the FEM. In this research, meshfree NS-PIM was combined with sequential linear analysis.

Sequentially linear analysis

Sequentially linear analysis (SLA) was first proposed by Rots (Rots 2001) with the aim of simplifying non-linear finite element analysis of concrete due to tension cracking. The locally brittle, snap-type response of many reinforced concrete structures inspired the idea to cap-

ture these events directly rather than trying to iterate around them with a Newton-Raphson scheme. SLA was based on the finite element re-analyzing of the structure at each cycle from an unloaded state, with the analysis following the secant modulus rather than the tangent. As such, the numerical difficulties typically encountered in tangent non-linear analysis, particularly in the softening part, were avoided, as the secant modulus is always positive.
Specifically, the non-linear analysis is substituted by a series of linear analyses, with the structure at each cycle slightly modified from the previous cycle. At each cycle, the element (or integration point) that is closest to cracking is identified. The following cycle analyses a structure with a crack at the element (or integration point), as identified in the previous cycle. The analysis is conducted according to the following steps (Rots and Invernizzi 2004; Rots et al. 2008).

a. The structure is loaded and analyzed with a normalized unit load.
b. The critical element closest to cracking is identified.
c. The load and analysis results are scaled to produce a crack at the critical element.
d. The structure is modified by changing the properties of the cracked element.
e. The previous steps are repeated, until the desired damage level is obtained.

Cracking

The final technical aspect relates to cracking. Cracking can be modeled discretely in both finite element and meshfree methods (Ngo, D. and Scordelis 1967; Rots and Blaauwendraad 1989), (ACI Report:446.3R-97 1997), where the crack tip stress and crack direction can be identified. The ability to model geometrically actual separation produces a numerical model that can accurately describe the actual cracking behavior. The main challenge (especially in three-dimensional bodies) with the discrete crack method is the need to continuously update the numerical model topology with the crack progression. Furthermore, a refined numerical model is required, particularly around the crack tip. The cost of conducting a discrete cracking analysis is large and, thus, mainly used for particularly detailed analysis of relatively small structures.

An alternative is the smeared crack method first introduction in 1968 by Rashid (Rashid 1968). It is currently widely used in finite element crack analysis mainly due to its numerical efficiency when compared to the discrete cracking method. This efficiency was achieved through maintaining the same geometric model and assuming that the actual crack effect can be distributed over the finite element width by changing the constitutive properties. This smearing effect is just an approximation of the actual discrete crack. In this approximation, some of the details are inevitably lost.

In addition to the above two methods, it is possible to use the extended FEM to model cracking. In this method, special enriching functions are added to the finite element approximation using the framework of partition of unity (Moës et al. 1999). In this approach, there is no need to modify the model topology with the crack propagation, as strong discontinuities can be modelled. However, the enrichment requires substantial numerical calculations that can slow the analysis.

The approach proposed herein uses the smeared method to model cracking. For such a model, it was previously observed that finite element results depend on element size (Bazant and Cedolin 1979; Bazant and Oh 1983; Cedolin and Bazant 1980). To maintain mesh objectivity and independence, Bazant and Cedolin (Bazant and Cedolin 1979),(Cedolin and Bazant

1980) proposed the concept of crack band width (h) to normalize the stress-strain curve with the aim of maintaining constant fracture energy.

Finally, two models exist to follow the crack development, the fixed and rotating crack models (Rots and Blaauwendraad 1989). In the first, it is assumed that the crack direction remains the same after its initiation, while in the second; the crack is allowed to change its direction with continuous change of stress state. In the approach proposed herein, the fixed crack model is employed.

Saw-tooth approximation

The application of SLA method to concrete is tightly linked to its tensile cracking. Many modeling options are available. One approach is to treat concrete as an ideal brittle material where the secant modulus of elasticity is instantly reduced to zero upon cracking. The results based of such a model will likely be mesh-dependent, as the crack fracture energy will not converge to the correct value upon mesh refinement (Bazant and Oh 1983). Alternatively, a gradual reduction of the secant stiffness in the softening part of the stress-strain curve will produce the saw-tooth approximation that is typically used in the SLA, Fig. 2.

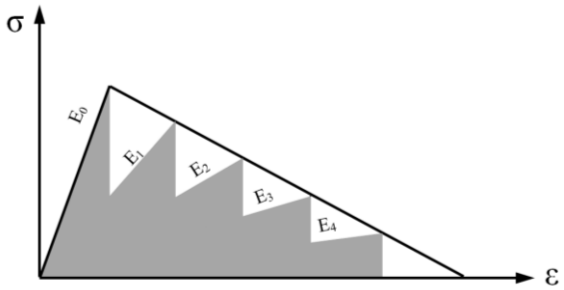

Fig. 2. Typical SLA curve.

The basic stress-strain curve can be modified to maintain the same fracture energy, which is related to the area under the softening stress-strain curve. The shaded area under the saw-tooth diagram is smaller than the total area under the stress-strain curve. To maintain constant fracture energy irrespective of the tooth count, the saw-tooth diagram needs to be adjusted. To achieve this, different regularized curves have been proposed (Rots and Invernizzi 2004; Rots et al. 2008). The most elegant was called Model C (Rots et al. 2008), which is based on a linear softening behavior and obtained by modifying both the tensile strength and ultimate tensile strain. The actual softening stress-strain curve is considered to represent the base value. Modified saw-tooth stresses are allowed to fluctuate around the base value within a specific band. For each tensile strength (f_{ti}), there is a larger value (f_{ti}^{+}) defining the maximum fluctuation limit and a smaller value (f_{ti}^{-}) defining the minimum fluctuation limit, Fig. 3. The resulting softening part can be generated as a series of secant lines, each with a progressively reduced tensile strength and slope and with a progressively increased maximum strain.

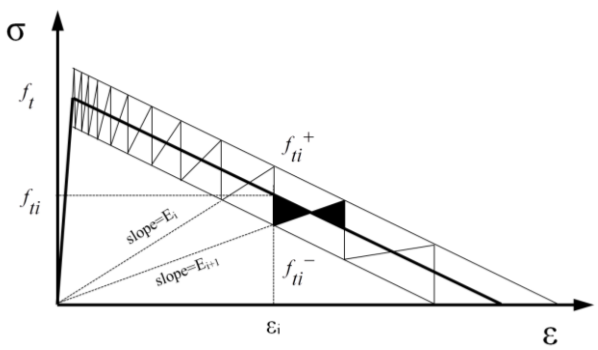

Fig. 3. Saw-tooth model C.

To regularize the softening behavior against the mesh size, the crack band width normalization concept was introduced by Bazant and Cedolin (Bazant and Cedolin 1979). Following that concept, Rots et al. (Rots and Invernizzi 2004; Rots et al. 2008) proposed using Eq. 8 to regularize the ultimate strain (ε_u) by relating it to the fracture energy (G_f), tensile strength (f_t), and crack band width (h):

$$\varepsilon_u = 2(G_f / h) / f_t \qquad (8)$$

The saw-tooth curve was constructed such that the value of f_{ti}^- for the last saw-tooth was equal to zero. This condition was set to maintain (in all practically) equal positive and negative areas above and below the actual stress-strain curve, to ensure constant total fracture energy.

In FEM, the value of the crack band width is related to the element size, element type, number of element integration points, and crack direction. The crack band width (h) can be expressed as:

Comment [1]: Since this relates to FEM do we need it. If so, please add a sentence relating it to the NS-PIM

$$h = h_{fac} . b \qquad (9)$$

where

h_{fac}: crack band width factor

b: element size

For simple plane strain triangles of regular uniform shape, where the cracks are parallel to the element side, it was found that the crack band width factor equals to 1.0 and that the element size is the element side length (Rots 1988).

The meshfree NS-PIM formulation implemented herein uses a linear shape function, as well as equal, regular, nodal spacing in both directions, with the cracks oriented mainly parallel to the nodal grid. For these conditions, it was found in the research herein that the equivalent element size is the nodal spacing and that a crack band width factor of 2.0 can produce the best overall results. This crack band width factor value can be related to the formulation of meshfree NS-PIM where the nodal stiffness is based on the support domain and a weak formulation. The stiffness matrix is calculated from the smoothed strains, as expressed in Eq. (7). These strains are calculated from the support nodes extending over the support domain. For the particular node of interest amongst a regular arrangement of nodes, this domain extends to a distance of twice the nodal spacing in each direction. The authors believe that this difference in the formulation of meshfree NS-PIM method based on the T3-scheme relative to the usual FEM formulation is the reason for the crack band width factor having a value of 2.0 rather than 1.0.

Numerical study

The meshfree NS-PIM method and its SLA implementation, as described above, were adopted in a new software code. The software, PISLA, has a graphical interface shown in Fig. 4 to allow the user to follow the analysis progress and present the results graphically. The progress of the load-deflection at any point is shown. The progress of cracks, stress, and deflection can also be selected by the user to be shown on the graphical interface. Maximum stress and deflection results are also presented numerically, as well as the time required to conduct the analysis. In this paper, all loads were assumed to be proportional. All the results reported herein were conducted using a computer with a 3.4 GHz Intel Core i7 CPU with 12 GB RAM.

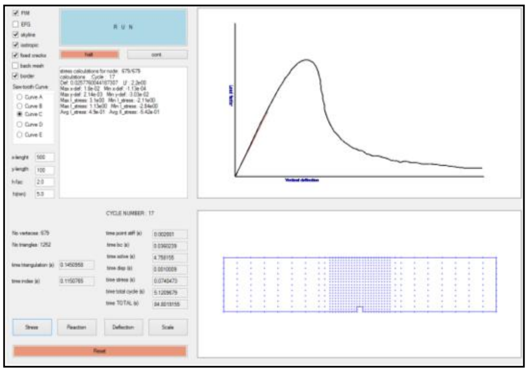

Fig. 4. Graphical user interface of PISLA.

To test the application of a meshfree method on SLA, a test beam model was used. The model was previously used by Rots et al. (Rots and Invernizzi 2004; Rots et al. 2008) to investigate the implementation of SLA with a finite element approach. The symmetric concrete beam was 500 mm long, with a 450 mm span, a 100 mm height, a 50 mm width, and a mid-span notch depth of 10 mm. Load was applied at the third-points of the free 450 mm span (Fig. 5). The maximum, constant, bending moment was generated within the beam's middle third.

The adopted material properties in this analysis were those used by Rots et al. (Rots and Invernizzi 2004; Rots et al. 2008): initial modulus of elasticity 38 GPa, initial tensile strength 3 MPa, and fracture energy 0.06 N mm/mm^2. The beam was modeled in its entirety, without any attempt to exploit its symmetry. Sensitivity of the saw-tooth model was tested by varying the number of teeth: 5, 10, 20, and 40; mesh sensitivity was tested by changing the nodal spacing: 20 mm, 10 mm, 5 mm, and 3.33 mm (Fig. 6); and the numerical models were refined mainly around the notched section.

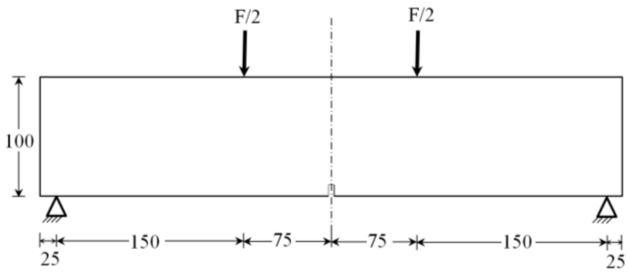

Fig. 5. Experimental notched concrete beam (23, 24).

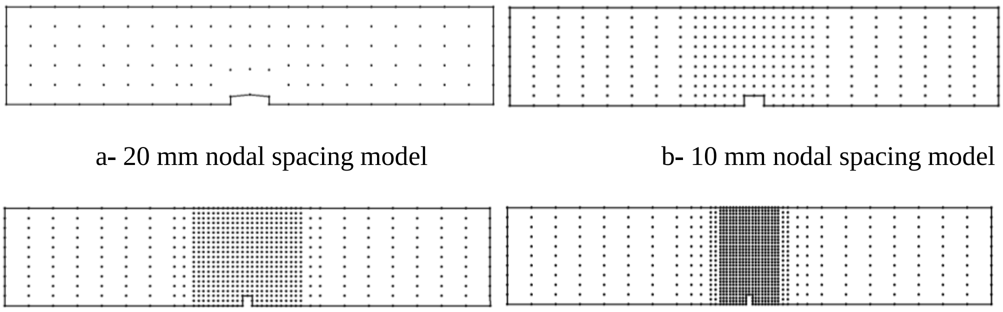

a- 20 mm nodal spacing model b- 10 mm nodal spacing model

c- 5 mm nodal spacing model d- 3.33 mm nodal spacing model

Fig. 6. The four numerical models analyzed.

Results

In the following sections, the analysis results from the different models are presented.

Base model

The base model had a nodal spacing of 10 mm and a saw-tooth with 20 teeth. The load-deflection curve of this model was constructed by linking the points resulting from the SLA (Fig. 7).

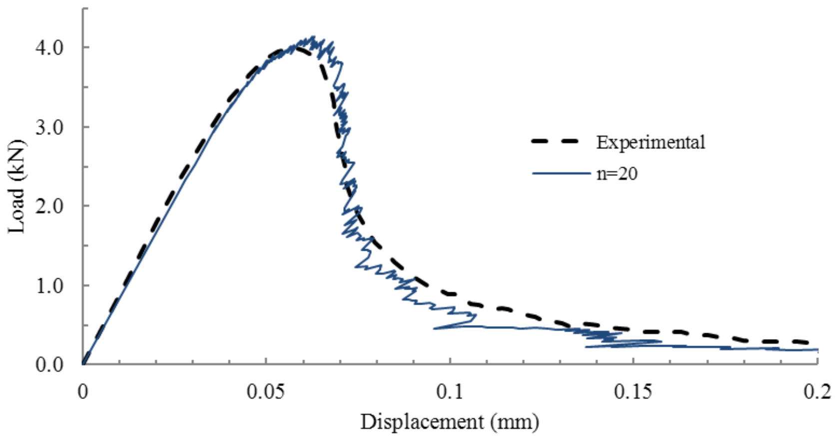

Fig. 7. Load-deflection results for the 10 mm nodal spacing model, 20 teeth.

The numerical results correlated well with the experimental behavior. The maximum numerical load was 4.14 kN, only 3.5% more than the maximum experimental value of 4.0 kN. The results were also found to be close to the results previously obtained using finite elements SLA with different saw-tooth curves and mesh densities (Rots and Invernizzi 2004; Rots et al. 2008).

The load-deflection curve resulting from current numerical method showed irregular behavior, particularly in the softening part. This behavior is associated with SLA method where damage is traced sequentially as it progresses through the structure. The irregular load-deflection behavior can be seen as a global reflection of damage represented on the local level by the saw-tooth approximation (Rots and Invernizzi 2004).

The presence of the notch resulted in cracking being limited to the area around the notch. The cracking progression, exaggerated deflection, and stress distribution in the central part of the beam are shown in Fig. 8. These results are shown at three stages of loading: 3.89 kN, 2.57 kN, and 0.27 kN, corresponding to cycle numbers 41, 195, and 341, respectively. All of these stages are in the softening part of behavior. In Fig. 8, the crack length is related to the saw-tooth number at the particular stage of cracking. The stress distribution is shown for the middle part of the beam, where the bending moment is constant.

At an early cracking stage, the cracks were nearly vertical and the stress distribution was nearly symmetric (Fig. 8-a). Early cracks appeared at the weakest section, corresponding to the notch location. With the cracking progression, the symmetry in cracking and stress distribution was lost. Theoretically symmetric results would have been expected. However, the presences of slight numerical approximations in the double precision calculations usually result in the loss of exact symmetry. There was no need to vary the section or material properties from one beam location to the other to break the symmetry, as done previously by some other researchers. The actual behavior of the physically tested model was similar due to slight imperfections in material properties, dimensions, support conditions, and/or loading positions.

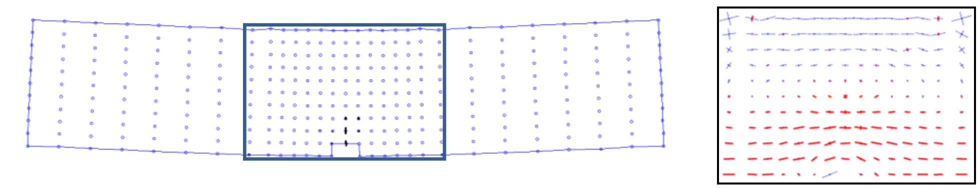

a- Crack pattern, exaggerated deflected shape, and principal stresses near mid-span at cycle 41 (load = 3.89 kN)

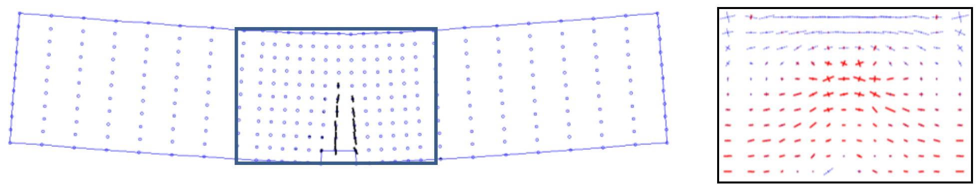

b- Crack pattern, exaggerated deflected shape, and principal stresses near mid-span at cycle 195 (load = 2.57 kN)

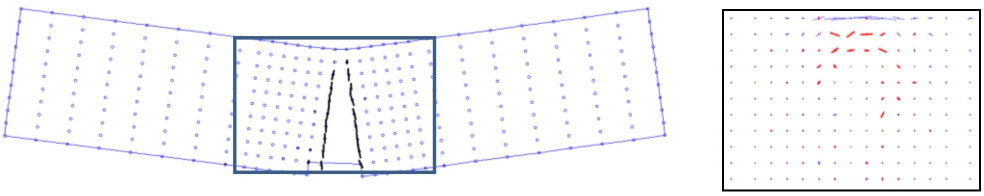

c- Crack pattern, exaggerated deflected shape, and principal stresses near mid-span at cycle 341 (load = 0.27 kN)

Fig. 8. Graphical outputs of the results of the 10 mm nodal spacing model with 20 teeth.

Fig. 8 shows clearly that the stress across the cracks reduced as the crack lengths increased. This behavior is related to the saw-tooth diagram, where f_{ti}^{+} reduced with the saw-tooth number of the crack, i as shown in Fig. 3.

The following sections present the results obtained from studying the effects of number of teeth in the saw-tooth model, nodal spacing, and node-distortion.

Effect of tooth count

Figure 9 shows the base model with 10 mm nodal spacing, the results for 5, 10, 20, and 40 teeth, where n indicates the number of teeth. The results were obtained for a crack band width factor of 2.0. Increasing the number of teeth improved the quality of results. The load-deflection curve became smoother and with less oscillation amplitude, as the number of teeth was increased. The overall average curve location remained stable, indicating similar fracture energy release. This behavior was expected and results from the more gradual release of fracture energy, as the number of teeth increases. However, this more refined behavior comes with a penalty in analysis time proportional to number of teeth.

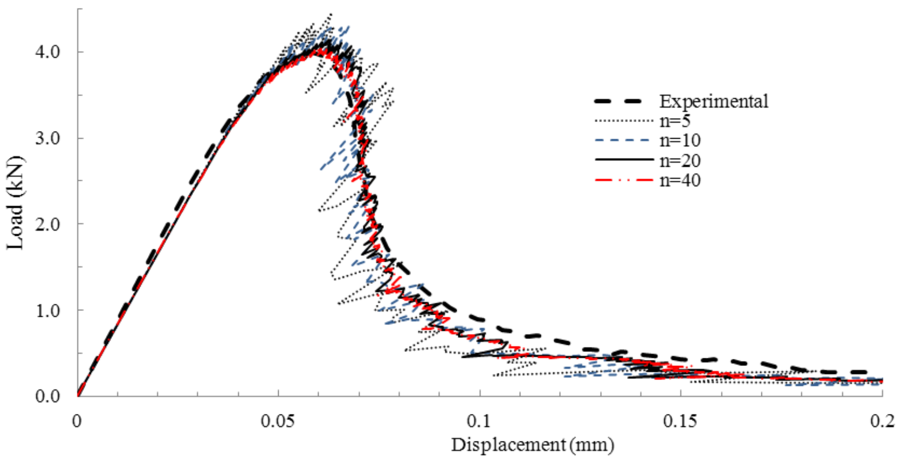

Fig. 9. Effect of number of teeth on the load-deflection results for the 10 mm nodal spacing.

The numerical peak load ranged from a high of 4.45 kN with 5 teeth to a low of 4.06 kN for 40 teeth, respectively (Fig. 9). This value decreased with an increase of teeth count, although at a reducing rate. This behavior reflects the saw-tooth model, in which the stress value oscillates above and below the base curve (Fig. 3). The oscillation amplitude reduces with tooth count. In this case, the model with 40 teeth was closest to the experimental value of 4.0 kN.

Effect of model refinement

Four models with nodal spacing of 20 mm, 10 mm, 5 mm, and 3.33 mm were tested (Fig. 6). The results obtained from these models for a saw-tooth model with 20 teeth are shown in Fig. 10. The results were obtained for a crack band width factor of 2.0. The meshfree method is known to produce results that are more flexible than the actual structure (Liu 2009). This trend was also observed in the current analysis. The initial slope of the numerical load-deflection curve was less than the experimental results. The numerical results converged to the test results, as the model was refined further. The very coarse 20 mm nodal spacing model showed rough and flexible behavior. There was, however, an overall similarity with the experimental behavior. Results of the other numerical models were closer to the experimental results. The peak load was predicted accurately by the 10 mm nodal spacing model, with a difference of 3.5% from the experimental results. The more refined 5 mm and 3.33 mm models predicted slightly higher peak values. Thus, the predicted behavior was still dependent, to a small degree, on nodal spacing. The maximum load resulting from the four nodal spacing was as little as 4.06 kN for the 20 mm nodal spacing to as much as 4.21 kN for the 3.33 mm nodal spacing.

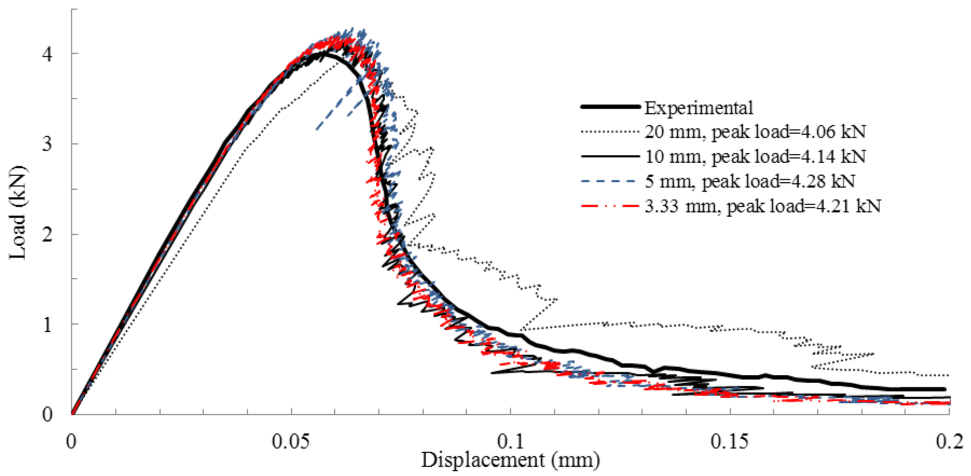

Fig. 10. Results of mesh refinement study, all results for 20 teeth.

This behavior relates to the tension cracking of concrete and the implications of using a smeared cracking method to model the actual cracks. In fracture mechanics, the energy released during the softening behavior per unit volume (or area) of concrete material is the fracture energy (G_f). In a meshfree (as well as finite element) analysis, the smeared crack is assumed to cover all of the smoothing domain (or element) regardless of the nodal spacing. Larger nodal spacing will result in the nodes (or elements) having larger fracture energy. To maintain constant value of fracture energy, regularization is used (Bazant and Cedolin 1979; Bazant and Oh 1983). One assumption of regularization is that the element can contain the material zone affected by the cracks, usually referred to as the FPZ (as described in section 1). The regularization scheme should work for any nodal spacing, as long as the spacing is larger than the FPZ width. One consequence of using a nodal spacing smaller than the FPZ width is that each node (or element) contained in the larger FPZ can dissipate the fracture energy. This numerical model will then overestimate the strength due to its ability to handle more fracture energy. This would explain the current results, with a slight anomaly for the 5 mm nodal spacing relative to those obtained from the 10 mm and 3.33 mm nodal spacing.

One possible reason is the fluctuating nature of the SLA analysis. Therefore, a single peak value is possibly not the best response measure. An average of many points around the peak result might be more appropriate. Overall, however, the softening behavior of the numerical models showed reasonable agreement with the experimental results. The generally similar overall behavior resulting from the four numerical models also indicates the accurate nodal stress values resulting from the meshfree NS-PIM analysis. This is one of the advantages of NS-PIM over the FEM approach with triangular elements (Liu 2009).

The analysis details of the four, studied, nodal spacings are shown in Table 1. The details including number of cycles, analysis time per cycle, total analysis time, and total analysis time expressed as a ratio relative to the total analysis time of the base model. From these results, it is clear that the analysis time of the most refined model, with 3.33 mm nodal spacing, was more than 41 times that required for the base model. Although more detailed results can be obtained from more refined models, the time penalty was disproportionally high. In this analysis, the 10 mm nodal spacing seems to provide a reasonable compromise between running time and level of result details. Notably the halving of the nodal spacing increases the total analysis time by more than an order of magnitude.

Table 1. Analysis details for different nodal spacing

Nodal spacing (mm)	No. of nodes	No. of analysis cycles	Analysis time/cycle (sec)	Total analysis time (sec)	Relative total analysis time
20	137	157	0.17	27	0.08
10	318	363	0.93	338	1 (reference)
5	679	823	4.81	3959	11.7
3.33	890	1213	11.55	14019	41.5

Effect of crack band width factor

To study the effect of changing the crack band width factor, the 3.33 mm nodal spacing model was used. The results obtained from various crack band width factors and 20 teeth saw-tooth model are shown in Fig. 11. The peak load values were as much as 4.21 kN and decreased to 4.08 kN, as the crack band width factors went from 2.0 to 2.3. There was a slight tendency of peak load reduction, as the crack band width factor increased. The general shape of the load-deflection curve was affected also, progressively dropping below the softening part of the experimental curve, as the factor value increased.

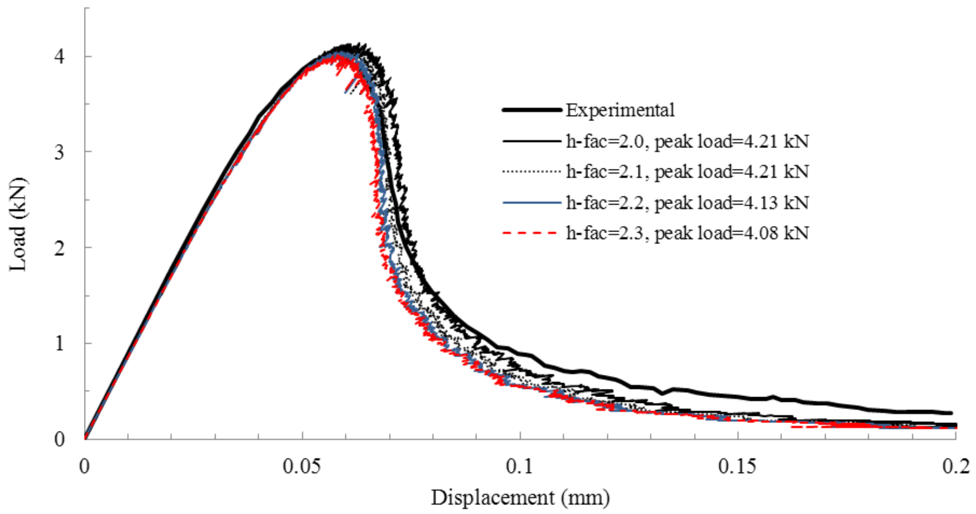

Fig. 11. Results of crack band width factor study.

For the specific problem presented in this research, with a nodal spacing of 10 mm, a crack band width factor of 2.0 worked well. For smaller nodal spacing, it is still possible to use that factor; however, the peak load will be overestimated slightly.

Sensitivity to nodal distortion

Finite element automatic mesh generators often produce irregular meshes. These can be distorted, particularly for complex geometries. In FEM, output accuracy is sensitive to element distortion. However, the meshfree method is known to be less sensitive to nodal distortion, (Liu 2009). To study the effect of nodal distortion on the accuracy of the results, the base model with 10 mm nodal spacing and 20 teeth was randomly distorted by ±10%, ±20%, ±30%, and ±40%, as shown in Fig. 12. The distortion was introduced by adding a random value within the appropriate range to the nodal coordinates. The random value was calculated by multiplying a pseudo random number in the range [-1, 1] by the nodal spacing and the specific distortion percentage.

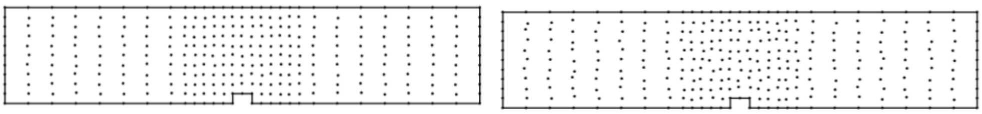

a- Mesh with ±10 distortion   b- Mesh with ±20 distortion

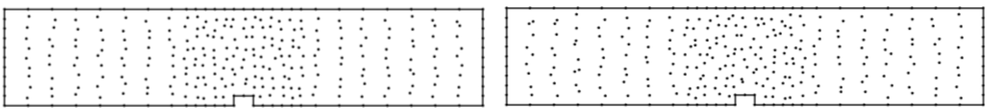

c- Mesh with ±30 distortion   d- Mesh with ±40 distortion

Fig. 12. Distorted models.

The initial stiffness for all the numerical models was similar regardless of distortion, thereby proving that the meshfree NS-PIM method is quite robust and insensitive to distortion. The peak loads ranged from 4.14 kN at no nodal distortion to 4.18 kN for a nodal distortion of ±40%. Furthermore, as shown in Figure 13, the overall shape of the numerical results was quite close to the experimental ones for distortion values up to ±20%. There was a trend of increased strength in the descending part of the curve with increased distortion. As the initial stiffness was unaffected by distortion, it is reasonable to relate the changed softening behavior to the effect of distortion on the crack band width, rather than the mesh free analysis. There are indications from the results that the peak load and the overall behavior are insensitive to nodal distortions. However, further work is required to establish solid conclusions in this regard.

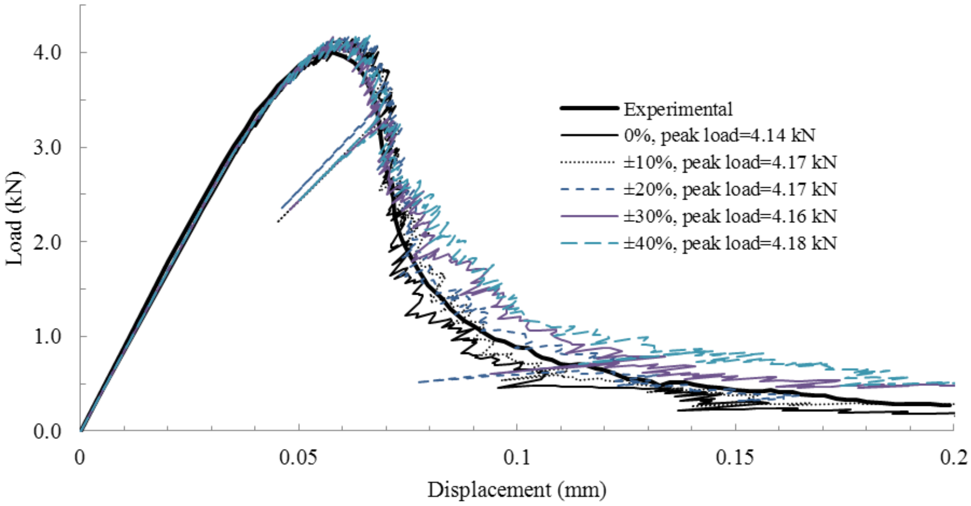

Fig. 13. Distorted model results.

Discussion

Since SLA is not currently supported in commercial FEM programs. So a direct comparison would be difficult to undertake. However, the general accuracy of results obtained from meshfree methods, was demonstrated by the current results. The method was quite stable within the range of the parameters studied. No numerical instability was encountered at any analysis stage.

One of the main issues of non-linear FEM, as well as finite element-based SLA, is the long analysis time. In both FEM and meshfree methods, output accuracy is related in part to the total number of degrees of freedom, hence the stiffness matrix size. As a comparison, the meshfree NS-PIM using the T3 scheme can produce more accurate stress results when compared with FEM using triangular elements (Liu 2009). The effect is directly reflected in SLA with its stress-based softening behavior. The other factor affecting SLA solution time is the total number of cycles. This number is the summation over all cracked nodes (integration points) of the last tooth number. Thus, there is an obvious advantage in reducing the total number of nodes to a level not affecting stress accuracy, as that will directly reduce the number of SLA analysis cycles. In this respect, meshfree NS-PIM can provide an advantage over comparable FEM approaches, however the exact correlations and comparisons need to be the subject of future studies.

Conclusions

Meshfree NS-PIM method was applied in the SLA analysis of cracking concrete. The method was used to analyze a notched concrete beam that was previously studied by Rots et al. (Rots and Invernizzi 2004; Rots et al. 2008) using finite element-based SLA. The meshfree SLA managed to produce numeric results that were close to experimental ones, namely the peak load and overall load-deflection behavior (including the softening part). The base model with 10 mm nodal spacing and 20 teeth predicted a peak load only 3.5% more than the experimental value, and increasing the number of teeth in the saw-tooth model produced a load-deflection curve that was more even and with less oscillation amplitude. The overall average location of the curves remained stable. However, there was an increase in the analysis time linearly related to the number of teeth in the saw-tooth mode.

What was also found was that in spite of maintaining equal fracture energy for the different numerical models with different nodal spacing, the results still depended slightly on nodal spacing. The normal crack band width factor value used in the analysis was 2.0. To maintain the same peak load output from the different models, the crack band width factor needs to be increased slightly with more refined models. More research is required to study this behavior.

Additionally, the numerical results were shown to be relatively insensitive to nodal spacing and model size. By reducing the nodal spacing by a factor of 6 from 20 mm to 3.33 mm, the peak load changed by less than 3.7%. This is an indication of the generally accurate stress results obtained from meshfree methods and the possibility of using smaller number of nodes to model large structures while still obtaining accurate results at the benefit of reduced analysis time. Furthermore, since the meshfree approach generates models that are less stiff than the actual structures, the displacements are not underestimated. Finally, and perhaps most importantly the predicted peak load was found to be insensitive to nodal distortions up to ±40%, and the overall behaviour insensitive to distortions of up to ±20%. Thus, there are two areas where a meshfree approach may hold strategic advantages over a FEM. The first is in the investigation of large deformation (in concrete, as well as other materials). The second is in the auto-generation of meshes from remote sensing data (e.g. laser scanning, photogrammetry). In such a case, the external geometry of an existing structure can be captured and transformed directly into a solid model. This could be of tremendous value in the assessment of older metal bridges and will be the subject of further study by the authors.

References

ACI Report:446.3R-97. (1997). *Finite Element Analysis of Fracture in Concrete Structures: State-of-the-Art*. 33.

Atluri, S. N., and Zhu, T. (1998). “A new Meshless Local Petrov-Galerkin (MLPG) approach in computational mechanics.” *Computational Mechanics*, 22(2), 117–127.

Bazant, Z. P., and Cedolin, L. (1979). “Blunt Crack Band Propagation in Finite Element Analysis.” *Journal of the Engineering Mechanics Division*, ASCE, 105(2), 297–315.

Bazant, Z. P., and Jirásek, M. (2002). “Nonlocal integral formulations of plasticity and damage: survey of progress.” *Journal of Engineering Mechanics*, (November).

Bazant, Z. P., and Oh, B. H. (1983). “Crack band theory for fracture of concrete.” *Materials and Structures, January-February*, 155–177.

Cedolin, L., and Bazant, Z. P. (1980). “EFFECT OF FINITE ELEMENT CHOICE IN BLUNT CRACK BAND ANALYSIS Luigi CEDOLIN.” 24, 305–316.

Chan, S. L. (1988). “Geometric and material non-linear analysis of beam-columns and frames using the minimum residual displacement method.” *International Journal for Numerical Methods in Engineering*, 26(12), 2657–2669.

Courant, R., Friedrichs, K. O., and Lewy, H. (1967). “On the partial difference equations of mathematical physics.” *IBM Journal*, vol. 11, 215 –235.

Crisfield, M. A. (1996). *Non-Linear Finite Element Analysis of Solids and Structures*. Wiley, 362.

Gingold, R. A., and Monaghan, J. J. (1977). “Smoothed particle hydrodynamics - Theory and application to non-spherical stars.” *Monthly Notices of the Royal Astronomical Society*, 181, 375–389.

Hillerborg, A., Modéer, M., and Petersson, P. E. (1976). “Analysis of crack formation and crack growth in concrete by means of fracture mechanics and finite elements.” *Cement and concrete research*.

Li, H., and Mulay, S. S. (2013). *Meshless Methods and Their Numerical Properties*. CRC Press, 447.

Liszka, T., and Orkisz, J. (1980). “The finite difference method at arbitrary irregular grids and its application in applied mechanics.” *Computers & Structures*, Il.

Liu, G. R., Zhang, G. Y., Dai, K. Y., Wang, Y. Y., Zhong, Z. H., Li, G. Y., and Han, X. (2005). “A linearly conforming point interpolation method (LC-PIM) for 2D solid mechanics problems.” *Int. J. Computer Methods*, 2(4), 645-665.

Liu, G. R. (2009). *Meshfree Methods: Moving Beyond the Finite Element Method, Second Edition*. CRC Press, 792.

Liu, G. R., and Zhang, G. Y (2013). *Smoothed Point Interpolation Methods: G space and weakened weak forms*, World Secientific Singapore.

Lucy, L. B. (1977). “A numerical approach to the testing of the fission hypothesis.” *The Astronomical Journal*, 82, 1013.

Moës, N., Dolbow, J., and Belytschko, T. (1999). “A finite element method for crack growth without remeshing.” *Int. J. Numer. Meth. Engng*, 46, 131–150.

Ngo, D. and Scordelis, A. C. (1967). “Finite Element Analysis of Reinforced Concrete Beams.” *Journal of ACI*, 64(3), 152–163.

Rashid, Y. R. (1968). “Ultimate strength analysis of prestressed concrete pressure vessels.” *Nuclear Engineering and Design*, 7(4), 334–344.

Riks, E. (1979). “An incremental approach to the solution of snapping and buckling problems.” *International Journal of Solids and Structures*, 15(7), 529–551.

Rots, J. G. (1988). “Computational modeling of concrete fracture.” Delft.

Rots, J. G. (2001). “Sequentially linear continuum model for concrete fracture.” *Fracture Mechanics of Concrete Structures*, G. P.-C. and J. G. M. van M. R. de Borst, J. Mazars, ed., A.A. Balkema, 831–839.

Rots, J. G., Belletti, B., and Invernizzi, S. (2008). “Robust modeling of RC structures with an ‘event-by-event’ strategy.” *Engineering Fracture Mechanics*, 75, 590–614.

Rots, J. G., and Blaauwendraad, J. (1989). “Crack models for concrete, discrete or smeared? Fixed, multi-directional or rotating?” *HERON*, 34(1).

Rots, J. G., and Invernizzi, S. (2004). “Regularized sequentially linear saw-tooth softening model.” *International Journal for Numerical and Analytical Methods in Geomechanics*, 28(78), 821–856.

Thomas, G. B., Weir, M. D., Hass, J., and Giordano, F. R. (2004). *Thomas' Calculus*. Addison Wesle, 1380.

Thomée, V. (2001). “From finite differences to finite elements.” *Journal of Computational and Applied Mathematics*, Elsevier Science Publishers B. V., 128(1-2), 1–54.